Article

Widespread six degrees Celsius cooling on land during the Last Glacial Maximum

https://doi.org/10.1038/s41586-021-03467-6

Received: 6 November 2020

Accepted: 17 March 2021

Published online: 12 May 2021

Check for updates

Alan M. Seltzer[1]✉, Jessica Ng[2], Werner Aeschbach[3], Rolf Kipfer[4,5,6], Justin T. Kulongoski[2], Jeffrey P. Severinghaus[2] & Martin Stute[7,8]

The magnitude of global cooling during the Last Glacial Maximum (LGM, the coldest multimillennial interval of the last glacial period) is an important constraint for evaluating estimates of Earth's climate sensitivity[1,2]. Reliable LGM temperatures come from high-latitude ice cores[3,4], but substantial disagreement exists between proxy records in the low latitudes[1,5–8], where quantitative low-elevation records on land are scarce. Filling this data gap, noble gases in ancient groundwater record past land surface temperatures through a direct physical relationship that is rooted in their temperature-dependent solubility in water[9,10]. Dissolved noble gases are suitable tracers of LGM temperature because of their complete insensitivity to biological and chemical processes and the ubiquity of LGM-aged groundwater around the globe[11,12]. However, although several individual noble gas studies have found substantial tropical LGM cooling[13–16], they have used different methodologies and provide limited spatial coverage. Here we use noble gases in groundwater to show that the low-altitude, low-to-mid-latitude land surface (45 degrees south to 35 degrees north) cooled by 5.8 ± 0.6 degrees Celsius (mean ± 95% confidence interval) during the LGM. Our analysis includes four decades of groundwater noble gas data from six continents, along with new records from the tropics, all of which were interpreted using the same physical framework. Our land-based result broadly supports a recent reconstruction based on marine proxy data assimilation[1] that suggested greater climate sensitivity than previous estimates[5–7].

The LGM is the most-recent extended period of globally stable climate that was substantially cooler than the present climate, and it therefore represents an important constraint for evaluating estimates of climate sensitivity from model simulations. The promise of LGM temperature reconstruction as a way of validating tools used to predict future warming relies on precise palaeotemperature reconstructions. However, efforts over recent decades to resolve global-mean LGM temperatures have produced widely varying results[1,5–7], in large part due to disagreements in low-latitude sea-surface cooling estimates that range from around 1 to 4 °C and the scarcity of high-confidence palaeotemperature records on land. Whereas high-elevation terrestrial records from the tropics have long indicated spatially consistent approximately 1-km lowering of LGM mountain snowlines associated with about 5–6 °C cooling[17–19], low-elevation palaeotemperature estimates from lake sediments[20–22] and pollen[23], for example, have suggested substantially less cooling. These disagreements have limited the use of LGM temperatures to inform our understanding of climate sensitivity.

Among existing terrestrial temperature proxies—each of which has different strengths and limitations—the 'noble gas palaeothermometer' has stood out since its introduction in the 1970s[24] as a promising tool for temperature reconstruction on land. This technique exploits the well-known temperature-dependent solubility functions[9,10] of neon (Ne), argon (Ar), krypton (Kr) and xenon (Xe) in water to quantitatively invert measured noble gas concentrations in ancient groundwater into past temperature at the water table (that is, the upper surface of the saturated zone) at the time of recharge[10,25,26]. Owing to the attenuation of seasonal temperature fluctuations in soil with depth, typical temperatures at the water table closely match mean annual ground surface temperatures (MAST), thus providing a direct physical link between MAST and noble gases dissolved in groundwater[10,25,26]. The potential of noble-gas-derived temperature (NGT) reconstruction is both far-reaching and firmly rooted in well-established physical principles, as a third of Earth's land area is estimated to hold LGM-aged groundwater[11] and noble gases are, by nature, inert and conservative tracers. To date, however, disparate approaches to groundwater dating and treatment of air bubble entrainment and dissolution among dozens of groundwater noble gas palaeotemperature studies have led to an inconclusive set of results. Although a handful of prominent tropical noble gas studies[13–16] have indicated a magnitude of low-elevation cooling during the LGM in line with the 5–6 °C implied by mountain snowline depression, the lack of a consistent approach and independent

[1]Marine Chemistry and Geochemistry Department, Woods Hole Oceanographic Institution, Woods Hole, MA, USA. [2]Geosciences Research Division, Scripps Institution of Oceanography, La Jolla, CA, USA. [3]Institute of Environmental Physics, Heidelberg University, Heidelberg, Germany. [4]Department of Water Resources and Drinking Water, Swiss Federal Institute of Aquatic Science and Technology, Eawag, Dübendorf, Switzerland. [5]Institute of Biogeochemistry and Pollutant Dynamics, Department of Environmental Systems Science, Swiss Federal Institute Technology, ETHZ, Zurich, Switzerland. [6]Institute of Geochemistry and Petrology, Department of Earth Sciences, Swiss Federal Institute Technology, ETHZ, Zurich, Switzerland. [7]Geochemistry Division, Lamont–Doherty Earth Observatory, Palisades, NY, USA. [8]Environmental Science Department, Barnard College, New York, NY, USA. ✉e-mail: aseltzer@whoi.edu

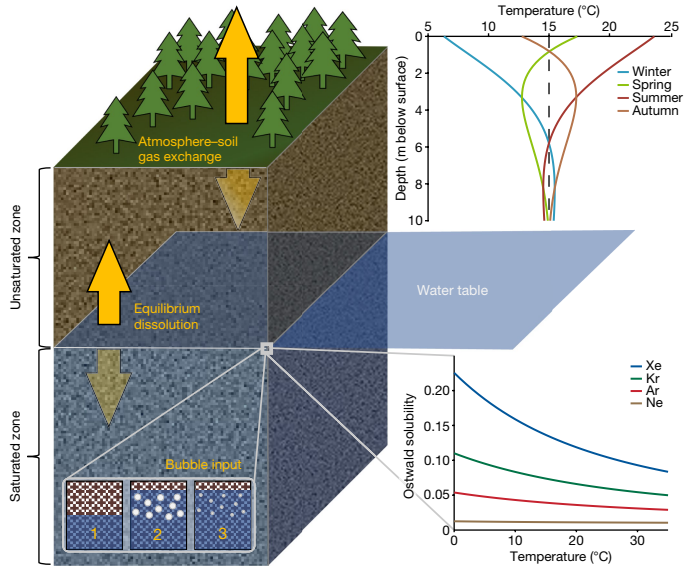

Fig. 1 | Overview of the noble gas palaeothermometer and its key components. Atmospheric gases enter soil pores in the unsaturated zone and dissolve into groundwater (salinity of around 0) at the water table, which typically lies below the minimum depth at which the soil temperature closely reflects the mean annual surface temperature (dashed black line). As shown in the bottom left cartoon, bubbles of soil air are entrained by the rising water table between stages 1 and 2 before partially dissolving under hydrostatic pressure between stages 2 and 3. Because groundwater is disconnected from soil air over time, owing to subsequent recharge and flow, its noble gas composition reflects conditions at the time of soil air dissolution and can be inverted to quantitatively resolve temperature using the well-known temperature-dependent solubility functions.

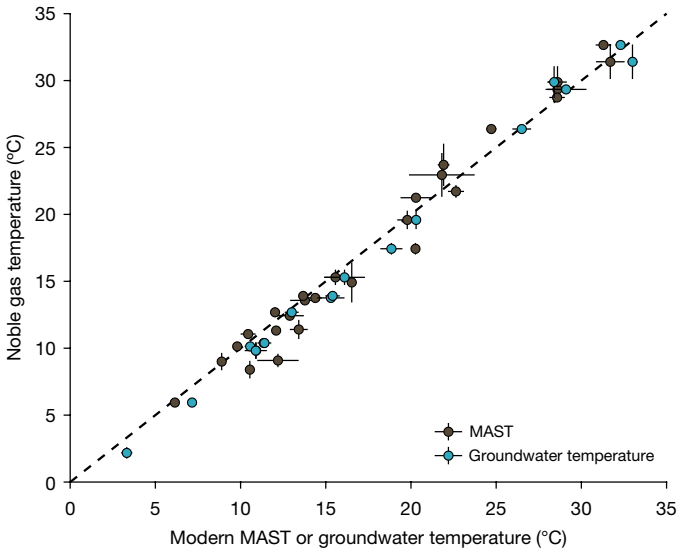

Fig. 2 | Noble gases in young groundwater accurately record modern temperatures. Comparison of error-weighted mean NGTs in Late Holocene groundwater ($n = 30$) with modern measured groundwater temperatures (blue circles) or MASTs (ERA5-Land upper soil temperatures) averaged from 1981 to 2019 (brown circles). Data are mean ± 1 s.e.m. and the dashed line indicates 1:1. The ERA5-Land temperature for the coldest sample is not shown because of ERA5-Land biases below 5 °C (Extended Data Fig. 2). Anthropogenic warming and Late Holocene temperature fluctuations may contribute slightly to scatter, but due to dating limitations and dispersive mixing we are unable to disentangle these effects.

validation of the noble gas technique has limited its wide adoption in climate studies.

Here, we combine the wealth of existing groundwater noble gas data with new measurements from key tropical locations to produce a composite global record of NGTs of the LGM. By comparing NGTs from young groundwater to modern MAST observations from 30 studies that range from around 2 to 33 °C, we evaluate the accuracy of NGTs and suitability of the various models commonly used to convert noble gas concentrations to temperature. Using the most robust NGT model, we then reconstruct low-and-mid-latitude LGM temperatures on land, compare our findings to previous efforts and discuss the broader implications for climate sensitivity.

Basis of the noble gas palaeothermometer

Four atmospheric noble gases (Ne, Ar, Kr and Xe) lack appreciable sinks or sources over glacial–interglacial timescales[27] and thus their concentrations dissolved in fresh water at solubility equilibrium—at a given temperature and barometric pressure—reflect well-understood physical constants that do not change with time. In groundwater, noble gases are acquired primarily via equilibrium dissolution of soil air at the water table, and secondarily by bubble entrainment and dissolution (Fig. 1). After shallow groundwater is isolated from overlying soil air by subsequent recharge or flow beneath a confining layer, dissolved Ne, Ar, Kr and Xe concentrations in groundwater are 'locked in' and affected only by dispersive mixing. Conveniently, for typical groundwater flow properties, mixing in the aquifer preserves oscillatory signals with periods on the order of thousands of years while damping higher-frequency signals, effectively acting as a natural low-pass filter[25]. In this sense, noble gases in groundwater that recharged around 20 thousand years (kyr) before present reflect long-term (millennial-scale) mean conditions at the water table during the LGM.

At a hypothetical site with a MAST of 15 °C and a seasonal cycle of ground surface temperatures of ±10 °C, temperatures at typical water table depths below around 10 m converge to within around 0.1 °C of MAST due to damping by the vertical diffusion of heat in soil[10,25,26] (Fig. 1). Therefore, after accounting for the contribution of bubble dissolution (or 'excess air'), measured noble gas concentrations in groundwater can be inverted to directly determine the MAST at the time and place of recharge, using their temperature-dependent solubility functions[9,10]. Although straightforward in principle, in practice many conceptual models have been proposed over recent decades to account for processes that may modify the composition of excess air or soil air at the water table[10,25,26]. Over the past twenty years, multiple theoretical, field and laboratory studies[28–30] have demonstrated the validity of the closed-system equilibration model[31], in which water table fluctuations entrain bubbles of soil air that partially dissolve under elevated hydrostatic pressure at solubility equilibrium. However, systematic reanalysis of noble gas measurements from young groundwater around the globe has not been carried out to assess the validity of the closed-system equilibration model and accuracy of NGTs in reconstructing modern temperatures, which is critical for establishing confidence in LGM temperature reconstructions.

Validation with modern groundwater

Using Late Holocene groundwater noble gas data (≤5 kyr recharge age) from 30 studies worldwide, we analysed each dataset using three common NGT models and compared error-weighted mean Late Holocene NGTs to both modern (1981–2019) ground surface temperatures (from ERA5-Land[32] reanalysis) and shallow (≤50 m) groundwater temperature measurements (Fig. 2). We find that the closed-system equilibration model considerably outperforms two other leading models[13,33] both in terms of accuracy and goodness of fit (Extended Data Fig. 1). The mean offset between NGTs from Late Holocene groundwater and ERA5-Land MAST in the closed-system equilibration model is negligible (<0.1 °C)

for MAST > 5 °C (n = 29), with a root-mean squared deviation (r.m.s.d.) of 1.4 °C. An evaluation of ERA5-Land temperatures against a global database of direct soil temperature measurements[34] shows similar scatter (r.m.s.d. = 1.6 °C) but no systematic bias for temperatures above 5 °C (Extended Data Fig. 2). Across the 16 studies for which groundwater temperatures within recharge areas were reported, Late Holocene NGTs from the closed-system equilibration model agree with measured groundwater temperatures with a r.m.s.d. of 1.1 °C, but display a mean offset of 0.7 °C (NGTs are systematically colder) that is probably due to slight geothermal warming of shallow groundwater. Taken together, our comparisons of modern groundwater NGTs to observations provide strong support for the accuracy of the closed-system equilibration model and suggest that cases in which the closed-system equilibration may fail to represent the physical system (for example, due to steady-state oxygen depletion in soil air[33,35]) are probably rare exceptions. The negligible mean offset between modern NGTs and MAST throughout this wide temperature range provides confidence in the use of groundwater noble gases as an unbiased palaeothermometer.

Consistent noble gas modelling approach

In view of both the fundamental physical arguments[28–31] and modern temperature validation that favour its use, we adopt the closed-system equilibration model to reconstruct LGM temperatures in 26 studies for which LGM-aged groundwater noble gas data exist. In previous studies, owing to the inherent challenges of dating groundwater with ^{14}C in dissolved inorganic carbon[36] or radiogenic ^{4}He[37], disparate approaches have been used to determine whether individual samples represent LGM recharge. Some studies include only those samples that fall within strict absolute age windows, others include only the coldest NGTs among samples of apparent Late Pleistocene age, and still others group samples that appear to represent the LGM because of a combination of cold NGTs and apparent age. These differences, along with varying choices of NGT models and solubility functions, have made it difficult to consistently compare the results of multiple studies.

Here, we define the LGM to be the coldest prolonged (multimillennial) interval of the last glacial period. We determine LGM cooling (ΔT_{LGM}) by subtracting Late Holocene weighted-mean NGTs (Fig. 2) from LGM NGTs determined using two distinct and plausible approaches, each applied uniformly across all datasets worldwide. Because apparent groundwater ages can suffer from large biases[26], and previous studies have deviated widely in correcting ^{14}C ages for the addition of ^{14}C-free carbon[36], we only consider samples for which the published ages are between 15 and 45 kyr to be candidate LGM samples. Then, in the first approach (AP1), we identify the coldest NGT within this range and include in our LGM estimate all other candidate samples with NGTs that agree within 1 °C, to determine a representative NGT from the set of coldest Late Pleistocene samples (multiple candidate samples exist in 23 out of 26 included studies). In the second approach (AP2), we divide the period from 15 to 45 kyr ago into six 5-kyr segments, identify the coldest segment, and then iteratively include all adjacent segments for which the error-weighted mean NGTs agree with the running-LGM estimate to within two standard deviations. We suggest that the first approach is the most robust, given that LGM NGTs are more likely to be biased to warmer temperatures. For example, a warm bias could be introduced because of (1) mixing with pre- or post-LGM groundwater; (2) permafrost-induced LGM recharge gaps; (3) correlated analytical errors that yield unphysical results with high temperature and excess air[38]; or (4) a possible widespread shift to grasslands vegetation during the LGM in regions that were forested or shrub covered in the Late Holocene[39] (which would lead to warming of LGM ground temperatures, relative to air temperatures[40]). Nonetheless, we find that the mean offset between LGM temperatures determined by these two approaches is around 0.9 °C, which is considerably smaller than the relevant approximately 5 °C range among previous estimates of low-latitude LGM cooling[1,5–7,13–23].

Whereas previous studies have reported only ΔT_{LGM} and its associated analytical uncertainties, here we explicitly estimate the total systematic error of groundwater noble-gas-based determinations of ΔT_{LGM}. In Extended Data Table 1, we identify four dominant sources of systematic error and quantify their respective magnitudes using simple physical models (Extended Data Fig. 3). We find that the two largest systematic errors—glacial–interglacial changes in recharge elevation and water table depth—are reduced by intrinsic compensating mechanisms. That is, for an unaccounted-for glacial–interglacial change in recharge elevation, the net bias in ΔT_{LGM} (assuming a typical lapse rate of approximately 6.5 °C km^{-1}) is reduced by roughly half due to associated changes in barometric pressure. For example, if the recharge area of a given aquifer shifted to a different location that was 100 m higher during the LGM, the corresponding LGM cooling bias of around 0.65 °C would be partially offset by the fact that lower barometric pressure leads to lower noble gas concentrations in groundwater and thus an approximately 0.28 °C higher NGT (Extended Data Fig. 3). Similarly, if an LGM water table was 20 m deeper than present and thus anomalously warmed by geothermal heat, the additional soil-air Kr and Xe acquired by gravitational settling[41,42] would also lead to a partially compensating cold bias. Across these groundwater datasets, most of which lie in nearly flat terrain with low-elevation recharge sites (Extended Data Table 2), we suggest that ±200 m and ±20 m conservatively represent the ranges of variability (±1σ) for glacial–interglacial shifts in recharge elevation and water table depth, respectively. With additional consideration of the smaller influences of absolute changes in LGM barometric pressure at fixed points on land[43] and mixing between groundwater of different recharge temperatures (see Methods), we estimate that a systematic uncertainty of ±0.9 °C (±1σ) must be taken into consideration, along with analytical uncertainties, when interpreting NGT-based reconstructions of ΔT_{LGM}.

Quantifying low-latitude cooling on land

In Fig. 3, we show ΔT_{LGM} estimates from 26 groundwater noble gas studies around the globe, including three new low-latitude records from Vietnam, India and Australia. We compare these noble-gas-based estimates to several influential previous efforts[1,5,7] to reconstruct low-and-mid-latitude sea surface temperatures. In addition to the direct physical coupling between temperatures at the land surface and water table (Fig. 1) that leads NGT to reliably record MAST (Fig. 2), numerical model experiments[44] have rigorously shown that equilibrium changes in water table temperature and mean annual surface air temperature (MAAT) in snow-free regions are equal to within around 0.2 °C. Therefore, a firm basis exists for inter-comparisons of MAST-based (that is, this study) and MAAT-based[1,7] ΔT_{LGM} analyses in the low latitudes. However, we note that at higher latitudes, decoupling of MAST and MAAT is possible due to changes in snow cover or vegetation[40], complicating the interpretation of high-latitude noble-gas-derived palaeotemperatures.

We find remarkable consistency in LGM cooling estimates from groundwater noble gas measurements between 45 °S and 35 °N (Fig. 3a). North of this latitude band, large regional differences arise from proximity to the great LGM ice sheets in the Northern Hemisphere, and permafrost gaps in LGM recharge lead to substantial zonal heterogeneity. Regional agreement among nearby groundwater records far from the ice sheets exemplifies the reproducibility of noble-gas-based temperature reconstructions. For example, ΔT_{LGM} estimates match closely across independent groundwater measurements from Namibia and Botswana; central and eastern China; Australia and New Zealand; the Mediterranean; and the southwestern USA (Fig. 3b). In low-latitude groundwater records between 45 °S and 35 °N (n = 15), we find an error-weighted mean ΔT_{LGM} of −5.8 ± 0.6 °C (mean ± 95% confidence interval, accounting for random and systematic error, and using approach AP1) (Fig. 3a). Each

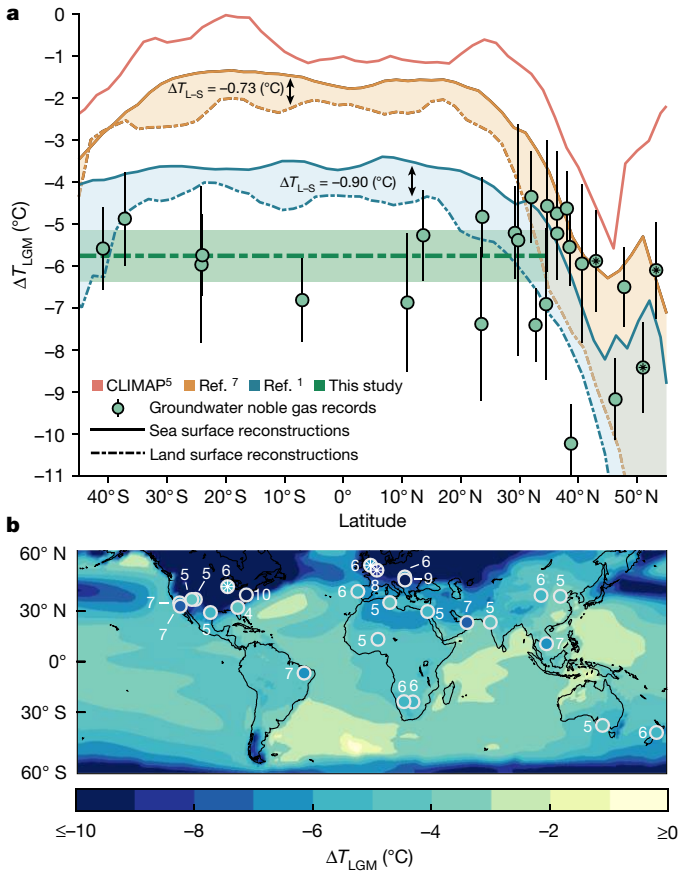

Fig. 3 | Noble gases suggest around 6 °C of low-elevation, low-latitude LGM cooling on land. a, Comparison by latitude of noble-gas-derived ΔT_{LGM} (this study, approach AP1) to zonal-mean land-surface (solid lines) and sea-surface (dashed lines) estimates of ΔT_{LGM} from key previous studies[1,5,7]. Data are mean ± 1 s.e.m. Our land-based mean of −5.8 ± 0.6 °C between 45° S and 35° N (thick green dashed line, with 95% confidence error envelope) partially overlaps the previously suggested range of cooling[1] (error of around ±0.3 °C), but it is incompatible with previous influential LGM temperature reconstructions[6,7,13] that have suggested less low-latitude cooling during the LGM and lower climate sensitivity. **b**, Map showing individual noble-gas-derived ΔT_{LGM} values (annotated points) superimposed on the data assimilation results of ref. [1] (plotted using the MATLAB Mapping Toolbox). Asterisks indicate sites with LGM recharge gaps.

of these low-latitude sites has a recharge elevation below 1.2 km, and the median recharge elevation is 375 m.

Our groundwater-based ΔT_{LGM} estimate over this latitude band is substantially colder than notable marine[5,7] and low-elevation terrestrial[8,21–23] reconstructions, but it is closer to the finding of a recent data assimilation study[1] as well as mountain snowline inferences of LGM cooling[17–19,45]. Regional mean values of LGM sea-surface cooling over these latitudes (weighted by area) from the CLIMAP project[5] (0.93 °C), a model–data hybrid[7] based on the MARGO global reconstruction of sea surface temperatures[6] (2.0 °C), and the recent data assimilation reconstruction[1] (3.75 °C) all fall below both our AP1 and AP2 (−4.8 ± 0.6 °C; Extended Data Fig. 5) estimates of LGM cooling on land. However, to directly compare land-surface and sea-surface cooling during the LGM, it is critical to consider the non-climatic impact of lower sea levels through the lapse rate on sea surface temperature, which is distinct from the climatic change at a fixed point on land. Whereas barometric pressure remains almost unchanged at a low-elevation fixed point on land during the LGM (Extended Data Fig. 4), the estimated increase in LGM sea-level pressure of around 15 hPa (ref. [43]) owing to a lower-than-present eustatic sea level of around 130 m leads to a non-climatic adiabatic sea-surface warming of around 0.85 °C (assuming a lapse rate of 6.5 °C km^{-1}) that is not experienced by low-latitude land surfaces. We find that the two above-mentioned model–data hybrid reconstructions of global LGM temperatures (Fig. 3a) show tropical mean land–sea differences in LGM cooling (ΔT_{L-S}) of −0.73 °C (ref. [7]) and −0.90 °C (ref. [1]), which are remarkably close to this expectation.

However, numerous model simulations of the global climatic response to elevated atmospheric carbon dioxide have found greater equilibrium warming over the continents than the oceans, linked by theory to changes to the hydrological cycle and the efficiency of latent cooling over land and sea surfaces[46–48]. We expect that this theory should also hold for cooling during the LGM. Thus, the observed ΔT_{L-S} in these LGM simulations is probably a consequence of a more complex set of processes than sea-level lowering alone. Although an incomplete understanding of land–sea cooling ratios during the LGM precludes a high-confidence translation of our terrestrial result into sea-surface cooling, our AP1 and AP2 ΔT_{LGM} estimates are incompatible with the CLIMAP and MARGO studies under even the most extreme suggested ratios of land-versus-sea surface temperature change (up to 1.8)[47,48]. Although we note that the land-surface cooling in the recent data assimilation study[1] is closer to our results (roughly in line with AP2 and around 1 °C less than AP1), the lack of terrestrial constraints in that analysis limits our ability to meaningfully interpret comparisons at the 1 °C level. Incorporation of these noble gas constraints into future model–data assimilation efforts may provide insights into the atmospheric dynamics that shaped ΔT_{L-S} during the LGM.

Climate sensitivity and next steps

Equilibrium climate sensitivity (ECS) is a widely adopted term that refers to the equilibrium response of Earth's global mean surface temperature to a doubling of atmospheric carbon dioxide[49]. This metric is particularly relevant to predicting the magnitude of future warming in response to anthropogenic greenhouse gas emissions. Estimates of ECS primarily come from Earth system model simulations and therefore palaeoclimate-based validation of these estimates is important[1,2], especially given the short instrumental record of the modern climate. The advent of new techniques for palaeoclimate data assimilation[50] using geochemical marine proxy data[1] has produced estimates of low-latitude LGM cooling that greatly exceed previous estimates that incorporated microfossil-assemblage-based transfer functions[5,6] and had provided a lower ECS than the model-based consensus[49]. Thus, in light of the fact that our low-latitude LGM cooling estimate is only compatible with a previous study[1] that suggested an ECS of 3.4 °C per doubling of atmospheric carbon dioxide (within the model-based range[49]), our study offers terrestrial proxy support for this recent reconciliation of proxy-based and model-based ECS estimates.

This work also enables future inter-proxy comparisons and calibrations on land, exploiting the strengths of noble gas palaeothermometry—such as the physical basis, mean annual rather than seasonal sensitivity and inherent low-pass filtering of noble gases (the primary weakness of noble gas palaeothermometry is poor age control). These strengths may aid in the interpretations of other terrestrial proxies that record higher-frequency climate signals and have more precise age control. Furthermore, our findings highlight the need for future work to fill large data gaps in the existing global record of groundwater NGTs, for instance through new measurements in South America or Southeast Asia. Future studies should also use the recent additions of noble gas palaeoclimate tools such as high-precision isotope measurements for palaeohydrology[41] and speleothem fluid inclusion measurements for cave palaeotemperatures[51] to provide new physically meaningful constraints on terrestrial palaeoclimate that may better inform regional hydroclimatic sensitivity to ongoing and future climate change.

Online content

Any methods, additional references, Nature Research reporting summaries, source data, extended data, supplementary information, acknowledgements, peer review information; details of author contributions and competing interests; and statements of data and code availability are available at https://doi.org/10.1038/s41586-021-03467-6.

1. Tierney, J. E. et al. Glacial cooling and climate sensitivity revisited. *Nature* **584**, 569–573 (2020).
2. Schmittner, A. et al. Climate sensitivity estimated from temperature reconstructions of the Last Glacial Maximum. *Science* **334**, 1385–1388 (2011).
3. Jouzel, J. et al. Orbital and millennial Antarctic climate variability over the past 800,000 years. *Science* **317**, 793–796 (2007).
4. Petit, J. R. et al. Climate and atmospheric history of the past 420,000 years from the Vostok ice core, Antarctica. *Nature* **399**, 429–436 (1999).
5. CLIMAP Project Members. The surface of the Ice-Age Earth. *Science* **191**, 1131–1137 (1976).
6. MARGO Project Members. Constraints on the magnitude and patterns of ocean cooling at the Last Glacial Maximum. *Nat. Geosci.* **2**, 127–132 (2009).
7. Annan, J. D. & Hargreaves, J. C. A new global reconstruction of temperature changes at the Last Glacial Maximum. *Clim. Past* **9**, 367–376 (2013).
8. Farrera, I. et al. Tropical climates at the Last Glacial Maximum: a new synthesis of terrestrial palaeoclimate data. I. Vegetation, lake-levels and geochemistry. *Clim. Dyn.* **15**, 823–856 (1999).
9. Jenkins, W. J., Lott, D. E. & Cahill, K. L. A determination of atmospheric helium, neon, argon, krypton, and xenon solubility concentrations in water and seawater. *Mar. Chem.* **211**, 94–107 (2019).
10. Kipfer, R., Aeschbach-Hertig, W., Peeters, F. & Stute, M. Noble gases in lakes and ground waters. *Rev. Mineral. Geochem.* **47**, 615–700 (2002).
11. Befus, K. M., Jasechko, S., Luijendijk, E., Gleeson, T. & Bayani Cardenas, M. The rapid yet uneven turnover of Earth's groundwater. *Geophys. Res. Lett.* **44**, 5511–5520 (2017).
12. Jasechko, S. et al. Global aquifers dominated by fossil groundwaters but wells vulnerable to modern contamination. *Nat. Geosci.* **10**, 425–429 (2017).
13. Stute, M. et al. Cooling of tropical Brazil (5 °C) during the Last Glacial Maximum. *Science* **269**, 379–383 (1995).
14. Weyhenmeyer, C. E. et al. Cool glacial temperatures and changes in moisture source recorded in Oman groundwaters. *Science* **287**, 842–845 (2000).
15. Stute, M., Schlosser, P., Clark, J. F. & Broecker, W. S. Paleotemperatures in the southwestern United States derived from noble gases in ground water. *Science* **256**, 1000–1003 (1992).
16. Kulongoski, J. T., Hilton, D. R. & Selaolo, E. T. Climate variability in the Botswana Kalahari from the late Pleistocene to the present day. *Geophys. Res. Lett.* **31**, L10204 (2004).
17. Porter, S. C. Snowline depression in the tropics during the last glaciation. *Quat. Sci. Rev.* **20**, 1067–1091 (2000).
18. Rind, D. & Peteet, D. Terrestrial conditions at the Last Glacial Maximum and CLIMAP sea-surface temperature estimates: are they consistent? *Quat. Res.* **24**, 1–22 (1985).
19. Klein, A. G., Seltzer, G. O. & Isacks, B. L. Modern and last local glacial maximum snowlines in the Central Andes of Peru, Bolivia, and Northern Chile. *Quat. Sci. Rev.* **18**, 63–84 (1999).
20. Tierney, J. E. et al. Northern Hemisphere controls on tropical southeast African climate during the past 60,000 years. *Science* **322**, 252–255 (2008).
21. Powers, L. A. et al. Large temperature variability in the southern African tropics since the Last Glacial Maximum. *Geophys. Res. Lett.* **32**, L08706 (2005).
22. Loomis, S. E. et al. The tropical lapse rate steepened during the Last Glacial Maximum. *Sci. Adv.* **3**, e1600815 (2017).
23. Bartlein, P. J. et al. Pollen-based continental climate reconstructions at 6 and 21 ka: a global synthesis. *Clim. Dyn.* **37**, 775–802 (2011).
24. Mazor, E. Paleotemperatures and other hydrological parameters deduced from noble gases dissolved in groundwaters; Jordan Rift Valley, Israel. *Geochim. Cosmochim. Acta* **36**, 1321–1336 (1972).
25. Stute, M. & Schlosser, P. in *Climate Change in Continental Isotopic Records* Vol. 78 (eds Swart, P. K. et al.) 89–100 (American Geophysical Union (AGU), 1993).
26. Aeschbach-Hertig, W. & Solomon, D. K. in *The Noble Gases as Geochemical Tracers* (ed. Burnard, P.) 81–122 (Springer, 2013).
27. Pepin, R. O. & Porcelli, D. Origin of noble gases in the terrestrial planets. *Rev. Mineral. Geochem.* **47**, 191–246 (2002).
28. Klump, S., Cirpka, O. A., Surbeck, H. & Kipfer, R. Experimental and numerical studies on excess-air formation in quasi-saturated porous media. *Wat. Resour. Res.* **44**, W05402 (2008).
29. Klump, S. et al. Field experiments yield new insights into gas exchange and excess air formation in natural porous media. *Geochim. Cosmochim. Acta* **71**, 1385–1397 (2007).
30. Aeschbach-Hertig, W., El-Gamal, H., Wieser, M. & Palcsu, L. Modeling excess air and degassing in groundwater by equilibrium partitioning with a gas phase. *Wat. Resour. Res.* **44**, W08449 (2008).
31. Aeschbach-Hertig, W., Peeters, F., Beyerle, U. & Kipfer, R. Palaeotemperature reconstruction from noble gases in ground water taking into account equilibration with entrapped air. *Nature* **405**, 1040–1044 (2000).
32. Hersbach, H. et al. The ERA5 global reanalysis. *Q. J. R. Meteorol. Soc.* **146**, 1999–2049 (2020).
33. Hall, C. M., Castro, M. C., Lohmann, K. C. & Ma, L. Noble gases and stable isotopes in a shallow aquifer in southern Michigan: implications for noble gas paleotemperature reconstructions for cool climates. *Geophys. Res. Lett.* **32**, L18404 (2005).
34. Chang, J. *Ground Temperature* (Blue Hill Meteorological Observatory, Harvard University, 1958).
35. Hall, C. M., Castro, M. C., Lohmann, K. C. & Sun, T. Testing the noble gas paleothermometer with a yearlong study of groundwater noble gases in an instrumented monitoring well. *Wat. Resour. Res.* **48**, W04517 (2012).
36. Han, L. F. & Plummer, L. N. A review of single-sample-based models and other approaches for radiocarbon dating of dissolved inorganic carbon in groundwater. *Earth Sci. Rev.* **152**, 119–142 (2016).
37. Aeschbach-Hertig, W., Stute, M., Clark, J. F., Reuter, R. F. & Schlosser, P. A paleotemperature record derived from dissolved noble gases in groundwater of the Aquia Aquifer (Maryland, USA). *Geochim. Cosmochim. Acta* **66**, 797–817 (2002).
38. Jung, M., Wieser, M., von Oehsen, A. & Aeschbach-Hertig, W. Properties of the closed-system equilibration model for dissolved noble gases in groundwater. *Chem. Geol.* **339**, 291–300 (2013).
39. Prentice, I. C., Harrison, S. P. & Bartlein, P. J. Global vegetation and terrestrial carbon cycle changes after the last ice age. *New Phytol.* **189**, 988–998 (2011).
40. Stute, M. & Sonntag, C. in *Isotopes of Noble Gases as Tracers in Environmental Studies* 111–122 (International Atomic Energy Agency, 1992).
41. Seltzer, A. M. et al. Deglacial water-table decline in Southern California recorded by noble gas isotopes. *Nat. Commun.* **10**, 5739 (2019).
42. Seltzer, A. M., Severinghaus, J. P., Andraski, B. J. & Stonestrom, D. A. Steady state fractionation of heavy noble gas isotopes in a deep unsaturated zone. *Wat. Resour. Res.* **53**, 2716–2732 (2017).
43. Mélières, M. A., Martinerie, P., Raynaud, D. & Lliboutry, L. Glacial–interglacial mean sea level pressure change due to sea level, ice sheet and atmospheric mass changes. *Global Planet. Change* **3**, 333–340 (1991).
44. Cey, B. D. On the accuracy of noble gas recharge temperatures as a paleoclimate proxy. *J. Geophys. Res.* **114**, D04107 (2009).
45. Broecker, W. S. & Denton, G. H. The role of ocean–atmosphere reorganizations in glacial cycles. *Geochim. Cosmochim. Acta* **53**, 2465–2501 (1989).
46. Manabe, S., Stouffer, R. J., Spelman, M. J. & Bryan, K. Transient responses of a coupled ocean–atmosphere model to gradual changes of atmospheric CO_2. Part I. annual mean response. *J. Clim.* **4**, 785–818 (1991).
47. Joshi, M. M., Gregory, J. M., Webb, M. J., Sexton, D. M. H. & Johns, T. C. Mechanisms for the land/sea warming contrast exhibited by simulations of climate change. *Clim. Dyn.* **30**, 455–465 (2008).
48. Sutton, R. T., Dong, B. & Gregory, J. M. Land/sea warming ratio in response to climate change: IPCC AR4 model results and comparison with observations. *Geophys. Res. Lett.* **34**, L02701 (2007).
49. Knutti, R. & Hegerl, G. C. The equilibrium sensitivity of the Earth's temperature to radiation changes. *Nat. Geosci.* **1**, 735–743 (2008).
50. Steiger, N. J., Hakim, G. J., Steig, E. J., Battisti, D. S. & Roe, G. H. Assimilation of time-averaged pseudoproxies for climate reconstruction. *J. Clim.* **27**, 426–441 (2014).
51. Ghadiri, E. et al. Noble gas based temperature reconstruction on a Swiss stalagmite from the last glacial–interglacial transition and its comparison with other climate records. *Earth Planet. Sci. Lett.* **495**, 192–201 (2018).

Methods

NGT fitting

Groundwater measurements (n = 753) of dissolved Ne, Ar, Kr and Xe abundances from 32 independent studies (Extended Data Table 2) were fitted to the closed-system equilibration model[31], partial re-equilibration model[13] and oxygen depletion model[33] using a non-linear least-squares solver ('lsqnonlin') in MATLAB. We excluded studies in which raw noble gas abundance data were unavailable, fewer than three noble gases were used for palaeotemperature reconstruction[52], major dating uncertainties precluded the identification of the LGM or in which the authors suggested that anomalous processes such as oxygen depletion[53] systematically decoupled the NGT from the MAST[54,55]. We also selected several representative modern-only NGT studies (that is, without LGM groundwater data) in which direct measurements of modern groundwater or ground surface temperatures were available[56,57], as a means of evaluating the accuracy of NGTs. As described in the main text, only the closed-system equilibration model was used for the ultimate calculation of LGM and Late Holocene recharge temperatures. For each model, the exact equations described in the literature were implemented, and values were directly compared for a test dataset with the software PANGA[58], demonstrating agreement to better than 0.01 °C. In each study, recharge pressures were calculated from published recharge elevations where available, and from the mean elevation over the study area for datasets in which no recharge elevation was provided. The latest solubility functions[9] for Ne, Ar, Kr and Xe were used for noble gas fitting, except for the cross-comparison with PANGA, in which the older solubility functions (as suggested previously[10] and used in PANGA) were implemented. A permissible entrapped air range (A) of 0–0.05 cm^3_{STP} (where STP indicates standard temperature and pressure) was used in the least-squares routine, as suggested previously[58], and fitted A values equal exactly to this maximum value were flagged and excluded, unless there was minimal dissolution (fractionation parameter $F \geq 0.95$).

Published noble gas measurement uncertainties were used for least-squares fitting in which provided (n = 685) and 1σ uncertainties of ±3%, ±2%, ±4% and ±4% were assumed for Ne, Ar, Kr, and Xe, respectively, when published errors were not provided (n = 68). NGT uncertainties for individual samples were calculated from the covariance matrix[58] produced by NGT fitting. For samples in which more than three gases were measured (n = 675), the system was overdetermined and thus goodness-of-fit could be assessed by calculating the reduced χ^2 value and determining the probability of randomly exceeding this value from the cumulative χ^2 distribution function with one degree of freedom. As described previously[58], we excluded all samples for which this probability was below 1% (n = 59), which indicates a very low likelihood that the closed-system equilibration model captures all of the processes that affect noble gas concentrations. For samples in which exactly three gases were measured (n = 78), uncertainties were determined by carrying out 100 Monte Carlo simulations per sample in which normally distributed perturbations (with a standard deviation given by the analytical uncertainty of each gas) were added to the measured values. Samples identified as problematic in their respective publications, for instance due to suspected measurement artefacts, sample collection or storage concerns, or extreme dating errors, were excluded from our final determination of LGM and Late Holocene temperatures. For each dataset, published recharge ages were used; otherwise, recharge age estimates suggested by the publication were followed (for example, translation of radiogenic ^{4}He to age using a ^{4}He accumulation rate suggested previously[59] or conversion of flow distances to recharge age based on a previously published relationship[15]).

After exclusion of published problematic samples and those with poor NGT model fit, Late Holocene recharge temperatures in each dataset were determined by calculating the weighed mean of all samples with recharge ages younger than 5 kyr. As described in the main text, weighted NGT means of LGM samples included by approaches AP1 and AP2 were calculated to estimate the mean LGM temperature in each dataset. ΔT_{LGM} was determined, for AP1 and AP2 separately, by subtracting the Late Holocene weighted-mean NGT from the weighted-mean AP1 and AP2 LGM NGTs, with errors determined using the quadrature sum of the respective Late Holocene and LGM NGT uncertainties. For datasets in which LGM-aged samples, but not Late Holocene samples (<5 kyr recharge age), were included (n = 2), ERA5-Land reanalysis temperatures were used, following the procedure for modern MAST determination described below.

Modern ground surface temperatures

To estimate modern MAST at the recharge sites of each included study, monthly mean ERA5-Land[32] upper soil temperatures (level 1: 0–7 cm), averaged from 1981 to 2019, were used in an algorithm to project modern temperature at the recharge elevation. For each study, first all ERA5-Land grid cells (0.1° × 0.1° resolution) within 1° latitude or longitude of the study area were identified and mean 1981–2019 ERA5-Land grid-cell temperatures were regressed against the natural log of mean surface pressure to determine an effective surface-temperature lapse rate in the region. This linear fit was then used to project the MAST at the surface pressure of the recharge site, and the uncertainty was estimated from the standard error of the regression line project to the recharge pressure. For evaluation of ERA5-Land temperatures, we carried out this same algorithm to estimate MAST at the elevations of published soil measurements in a global database[34].

New data

This study includes new (previously unreported) noble gas data from groundwater samples collected in the mid-1990s in Australia and Vietnam, and between 2008 and 2010 in India. These samples were analysed at either the Lamont–Doherty Earth Observatory or Heidelberg University. The Australian groundwater samples (n = 29) were analysed at Lamont–Doherty and were collected from a deep sandstone aquifer in South Australia (around 37.2° S 140.8° E) with 100–120 m recharge elevation. The Vietnamese groundwater samples (n = 23) were collected from a deep sedimentary aquifer near Ho Chi Minh City (around 10.9° N 106.6° E) with a recharge elevation of approximately 50 m and were measured at Lamont–Doherty. The Indian groundwater samples (n = 76) were collected from a confined sedimentary aquifer in Cambay Basin (Gujarat, India, around 23° N 72° E) with a low recharge elevation (about 50–150 m) and measured for noble gas abundances at Heidelberg. All groundwater samples from these sites were dated with ^{14}C of dissolved inorganic carbon and samples with detectable 'bomb' carbon (^{14}C activity > 100% modern carbon[60]) were assumed modern and assigned a recharge age of zero. All relevant site information (for example, geographical coordinates, modern surface and groundwater temperatures, recharge elevations, groundwater ages), noble gas measurements, and analytical uncertainties are included in the associated dataset and code package.

Atmospheric pressure on land during the LGM

We developed a simple box model to estimate the pressure at a fixed point in the atmosphere during the LGM. In this model, global changes in the total mass and distribution of atmospheric air are determined by accounting for lowering of global-mean sea level and temperature during the LGM and the growth of ice sheets with a mean altitude of 2 km at high latitudes. Our model accounts for the loss of air (approximated as N_2 and O_2) by dissolution into an approximately 3 °C cooler mean ocean[61] and occlusion in glacial ice bubbles (around 10% by volume), and assumes a mean LGM cooling at (modern) eustatic sea level of 6 °C. We assume a uniform 6.5 °C km^{-1} lapse rate for simplicity, although we find that the change in LGM pressure is insensitive to even 50% changes in LGM lapse rate or global MAST. The simplified barometric equation for a constant lapse rate is used to calculate

the change in pressure with elevation in the LGM atmosphere, after accounting for whole-atmosphere mass changes. We find that absolute LGM-versus-modern changes in atmospheric pressure at low elevation are negligible, although the cooling of the atmosphere and displacement of air by ice sheets leads to slightly larger changes in pressure at high elevation (Extended Data Fig. 3). Although we find that atmospheric pressure changes are negligible at fixed low elevations (that is, on land), the global mean sea-level pressure increases by around 0.015 atm (in line with a previous study[43]) owing to the approximately 130-m absolute lowering of the eustatic sea level during the LGM, thereby leading to lapse-rate-induced non-climatic warming that does not affect low-elevation land surfaces.

Sensitivity tests

To quantify the overall systematic error associated with noble gas palaeothermometry, we identified leading sources of systematic error and developed simple physical models to determine their respective magnitudes (Extended Data Table 1, Extended Data Fig. 4). In each case, we begin with a control experiment at a recharge elevation of 1 km with a MAST of 10 °C at the ground surface and water table, where dissolved noble gas concentrations are in equilibrium with atmospheric air. The sensitivity of NGTs to an unaccounted-for shift in recharge elevation was tested by determining the equilibrium noble gas concentrations in water equilibrated at higher or lower elevation (and thus higher or lower surface pressures and MASTs, assuming a 6.5 °C km^{-1} lapse rate), and using these concentrations to calculate NGTs using the closed-system equilibration model prescribed with the original (1 km elevation) surface pressure. The magnitude of the NGT bias (T') was determined from the difference between calculated NGTs and the 10 °C original recharge temperature. The total recharge-elevation sensitivity was estimated from T' values associated with a ±200-m shift in recharge elevation. The sensitivity of NGTs to water table depth was assessed by determining equilibrium groundwater Ne, Ar, Kr and Xe concentrations in water at a shallower or deeper water table that was warmer or cooler (via an assumed geothermal gradient of 30 °C km^{-1}) and above which noble gas concentrations were either enriched or depleted by gravitational enrichment[62] based on their elemental mass difference from mean air (29 g mol^{-1}). By similarly using the closed-system equilibration model (assuming atmospheric, and not gravitationally fractionated, air composition) to calculate NGTs, the associated water table depth bias in NGT was determined from the difference of modelled NGTs for a 20-m deeper or shallower water table from the starting recharge temperature (10 °C). The sensitivity of NGTs to small unaccounted-for LGM changes in barometric pressure (<1% at elevations below 3 km) (Extended Data Fig. 3) was determined by calculating equilibrium concentrations of Ne, Ar, Kr and Xe in equilibrium with air at higher and lower pressures, and then using these concentrations to constrain the closed-system equilibration model prescribed with the starting recharge pressure. The associated NGT bias was again determined by subtracting NGTs from the 10 °C starting recharge temperature, and a value of 1% was assumed to represent the maximum plausible LGM change in recharge pressure. Finally, the sensitivity of NGTs to mixing was estimated by determining the NGTs of equal-parts binary mixtures between the starting groundwater composition and air-equilibrated groundwater ranging in recharge temperature from 0 to 20 °C. By subtracting NGTs from the mean temperature of these binary mixtures, the NGT bias due to mixing was determined, and a mixing end-member range of ±5 °C (that is, mixing of 15 °C or 5 °C water with the 10 °C groundwater in this example) was assumed to represent the most extreme plausible mixing scenarios.

Data availability

All original groundwater data (noble gas concentrations, ages, water temperatures (if available)), recharge elevations, study locations, fitted parameters and statistical uncertainties are freely available for download through PANGAEA (https://doi.org/10.1594/PANGAEA.929176). NGT time series plots of each study are available as supplementary files. Source data are provided with this paper.

Code availability

All MATLAB scripts for NGT fitting (including documentation) are freely available from zenodo (https://doi.org/10.5281/zenodo.4589442).

52. Heaton, T. H. E., Talma, A. S. & Vogel, J. C. Dissolved gas paleotemperatures and ^{18}O variations derived from groundwater near Uitenhage, South Africa. *Quat. Res.* **25**, 79–88 (1986).
53. Freundt, F., Schneider, T. & Aeschbach-Hertig, W. Response of noble gas partial pressures in soil air to oxygen depletion. *Chem. Geol.* **339**, 283–290 (2013).
54. Castro, M. C., Hall, C. M., Patriarche, D., Goblet, P. & Ellis, B. R. A new noble gas paleoclimate record in Texas—basic assumptions revisited. *Earth Planet. Sci. Lett.* **257**, 170–187 (2007).
55. Ma, L., Castro, M. C. & Hall, C. M. A late Pleistocene–Holocene noble gas paleotemperature record in southern Michigan. *Geophys. Res. Lett.* **31**, L23204 (2004).
56. Masbruch, M. D., Chapman, D. S. & Solomon, D. K. Air, ground, and groundwater recharge temperatures in an alpine setting, Brighton Basin, Utah. *Wat. Resour. Res.* **48**, W10530 (2012).
57. Saraceno, J., Kulongoski, J. T. & Mathany, T. M. A novel high-frequency groundwater quality monitoring system. *Environ. Monit. Assess.* **190**, 477 (2018).
58. Jung, M. & Aeschbach, W. A new software tool for the analysis of noble gas data sets from (ground)water. *Environ. Model. Softw.* **103**, 120–130 (2018).
59. Clark, J. F., Stute, M., Schlosser, P., Drenkard, S. & Bonani, G. A tracer study of the Floridan Aquifer in southeastern Georgia: implications for groundwater flow and paleoclimate. *Wat. Resour. Res.* **33**, 281–289 (1997).
60. Stuiver, M. & Polach, H. A. Reporting of ^{14}C data. *Radiocarbon* **19**, 355–363 (1977).
61. Bereiter, B., Shackleton, S., Baggenstos, D., Kawamura, K. & Severinghaus, J. Mean global ocean temperatures during the last glacial transition. *Nature* **553**, 39–44 (2018).
62. Schwander, J. in *The Environmental Record in Glaciers and Ice Sheets* (eds Oeschger, H. & Langway, C. C.) 53–67 (Wiley, 1989).
63. Andrews, J. N. & Lee, D. J. Inert gases in groundwater from the Bunter Sandstone of England as indicators of age and palaeoclimatic trends. *J. Hydrol.* **41**, 233–252 (1979).
64. Stute, M., Clark, J. F., Schlosser, P., Broecker, W. S. & Bonani, G. A. 30,000 yr Continental paleotemperature record derived from noble gases dissolved in groundwater from the San Juan Basin, New Mexico. *Quat. Res.* **43**, 209–220 (1995).
65. Beyerle, U. et al. Climate and groundwater recharge during the last glaciation in an ice-covered region. *Science* **282**, 731–734 (1998).
66. Clark, J. F., Davisson, M. L., Hudson, G. B. & MacFarlane, P. A. Noble gases, stable isotopes, and radiocarbon as tracers of flow in the Dakota aquifer, Colorado and Kansas. *J. Hydrol.* **211**, 151–167 (1998).
67. Kulongoski, J. T., Hilton, D. R., Izbicki, J. A. & Belitz, K. Evidence for prolonged El Niño-like conditions in the Pacific during the Late Pleistocene: a 43 ka noble gas record from California groundwaters. *Quat. Sci. Rev.* **28**, 2465–2473 (2009).
68. Seltzer, A. M., Stute, M., Morgenstern, U., Stewart, M. K. & Schaefer, J. M. Mean annual temperature in New Zealand during the last glacial maximum derived from dissolved noble gases in groundwater. *Earth Planet. Sci. Lett.* **431**, 206–216 (2015).
69. Zhu, C. & Kipfer, R. Noble gas signatures of high recharge pulses and migrating jet stream in the late Pleistocene over Black Mesa, Arizona, United States. *Geology* **38**, 83–86 (2010).
70. Edmunds, W. M., Ma, J., Aeschbach-Hertig, W., Kipfer, R. & Darbyshire, D. P. F. Groundwater recharge history and hydrogeochemical evolution in the Minqin Basin, North West China. *Appl. Geochem.* **21**, 2148–2170 (2006).
71. Kreuzer, A. M. et al. A record of temperature and monsoon intensity over the past 40 kyr from groundwater in the North China Plain. *Chem. Geol.* **259**, 168–180 (2009).
72. Stute, M. & Deak, J. Environmental isotope study (^{14}C, ^{13}C, ^{18}O, D, noble gases) on deep groundwater circulation systems in Hungary with reference to paleoclimate. *Radiocarbon* **31**, 902–918 (1989).
73. Beyerle, U. et al. Evidence for periods of wetter and cooler climate in the Sahel between 6 and 40 kyr BP derived from groundwater. *Geophys. Res. Lett.* **30**, 1173 (2003).
74. Varsányi, I., Palcsu, L. & Kovács, L. Ó. Groundwater flow system as an archive of palaeotemperature: noble gas, radiocarbon, stable isotope and geochemical study in the Pannonian Basin, Hungary. *Appl. Geochem.* **26**, 91–104 (2011).
75. Corcho Alvarado, J. A. et al. European climate variations over the past half-millennium reconstructed from groundwater. *Geophys. Res. Lett.* **36**, L15703 (2009).
76. Blaser, P. C. et al. A 40 ka record of temperature and permafrost conditions in northwestern Europe from noble gases in the Ledo-Paniselian Aquifer (Belgium). *J. Quat. Sci.* **25**, 1038–1044 (2010).
77. Klump, S., Grundl, T., Purtschert, R. & Kipfer, R. Groundwater and climate dynamics derived from noble gas, ^{14}C, and stable isotope data. *Geology* **36**, 395–398 (2008).
78. Stute, M. & Talma, A. Glacial temperatures and moisture transport regimes reconstructed from noble gases and $\delta^{18}O$, Stampriet aquifer, Namibia. In *Isotope Techniques in the Study of Past and Current Environmental Changes in the Hydrosphere and the Atmosphere* 307–328 (1998).
79. Carreira, P. M. *Paleoáguas de Aveiro* (Universidade de Aviero, 1998).
80. Sundal, A., Brennwald, M. S., Aagaard, P. & Kipfer, R. Noble gas composition and $^{3}H/^{3}He$ groundwater ages in the Gardermoen Aquifer, Norway: improved understanding of flow dynamics as a tool for water management. *Sci. Total Environ.* **660**, 1219–1231 (2019).
81. Trabelsi, R., Matsumoto, T., Zouari, K., Trabelsi, M. & Kumar, B. Investigation of paleoclimate signatures in Sfax deep groundwater (Southeastern Tunisia) using environmental isotopes and noble gases. *Quat. Int.* **547**, 208–219 (2020).

82. Abouelmagd, A. et al. Paleoclimate record in the Nubian Sandstone Aquifer, Sinai Peninsula, Egypt. *Quat. Res.* **81**, 158–167 (2014).
83. Wieser, M. *Imprints of Climatic and Environmental Change in a Regional Aquifer System in an Arid Part of India using Noble Gases and Other Environmental Tracers* (University of Heidelberg, 2011).
84. Wieser, M., Aeschbach-Hertig, W., Schneider, T., Deshpande, R. D. & Gupta, S. K. A temperature and monsoon record derived from environmental tracers in the groundwater of northwest India. In *International Symposium on Isotopes in Hydrology, Marine Ecosystems and Climate Change Studies* 7–14 (International Atomic Energy Agency, 2013).

Acknowledgements We thank the entire community of groundwater noble gas geochemists, particularly the pioneers E. Mazor and J. N. Andrews, for decades of careful work in analysing groundwater from around the world and furthering our physical understanding of inert gases in groundwater; A. Moulla and T. Condesso de Melo for sharing data, and D. Bekaert for helpful discussions. The manuscript was improved by helpful suggestions from A. Manning, J. Clark and David McGee. This work was supported in part by NSF-EAR-1702704, NSF-EAR-1702571, and NSF-OCE-1923915.

Author contributions A.M.S. wrote the manuscript and carried out modelling and data analysis. J.N. and A.M.S. created the database. J.P.S. developed the LGM atmospheric pressure model. A.M.S., J.N., W.A., M.S., J.T.K. and R.K. contributed groundwater datasets, all authors contributed to weekly discussions about data interpretation and modelling. All authors edited and revised the manuscript.

Competing interests The authors declare no competing interests.

Additional information

Supplementary information The online version contains supplementary material available at https://doi.org/10.1038/s41586-021-03467-6.

Correspondence and requests for materials should be addressed to A.M.S.

Peer review information *Nature* thanks Jordan Clark, Andrew Manning, David McGee and the other, anonymous, reviewer(s) for their contribution to the peer review of this work. Peer reviewer reports are available.

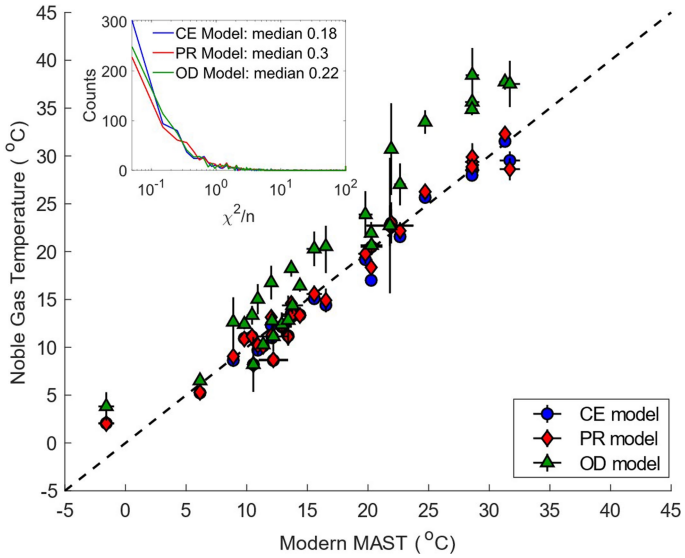

Extended Data Fig. 1 | Evaluation of leading noble gas models. Comparison of Late Holocene NGTs to ERA5-Land 1981–2019 MASTs across three NGT models and χ^2 goodness-of-fit histogram comparison of all groundwater samples (n = 753) included in this work (normalized by degrees of freedom, n) (inset). The closed-system equilibration (CE) model agrees closest with ERA5-Land temperatures (r.m.s.d. = 1.4 °C), followed by the partial re-equilibration (PR) (r.m.s.d. = 1.5 °C) and oxygen depletion (OD) (r.m.s.d. = 5.7 °C) models. The closed-system equilibration model also exhibits the best goodness-of-fit (lowest median χ^2/n). Data are mean ± 1 s.e.m.

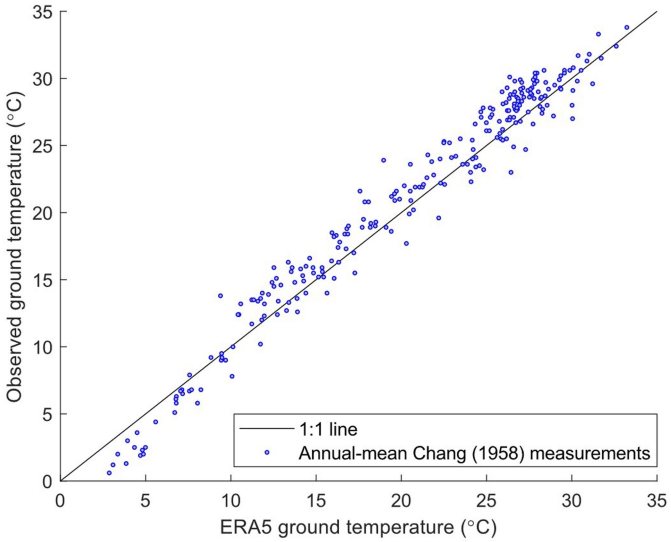

Extended Data Fig. 2 | ERA5-Land temperatures are unbiased above 5 °C. Comparison of 1981–2019 mean annual ERA5-Land ground (upper soil) temperatures to a global database of modern mean annual measured ground temperatures[34], using the approach described in the Methods to project ERA5-Land temperatures to the observation elevations. Whereas below approximately 5 °C, ERA5-Land temperatures appear to be systematically biased to be warmer than the observed temperature, above 5 °C they consistently overlap the 1:1 line with an r.m.s.d. of 1.6 °C. Observed temperatures tend to be slightly warmer than ERA5-Land temperatures on average, perhaps because of the typical locations of micrometeorological stations in barren fields, with little cooling from the shade provided by vegetation.

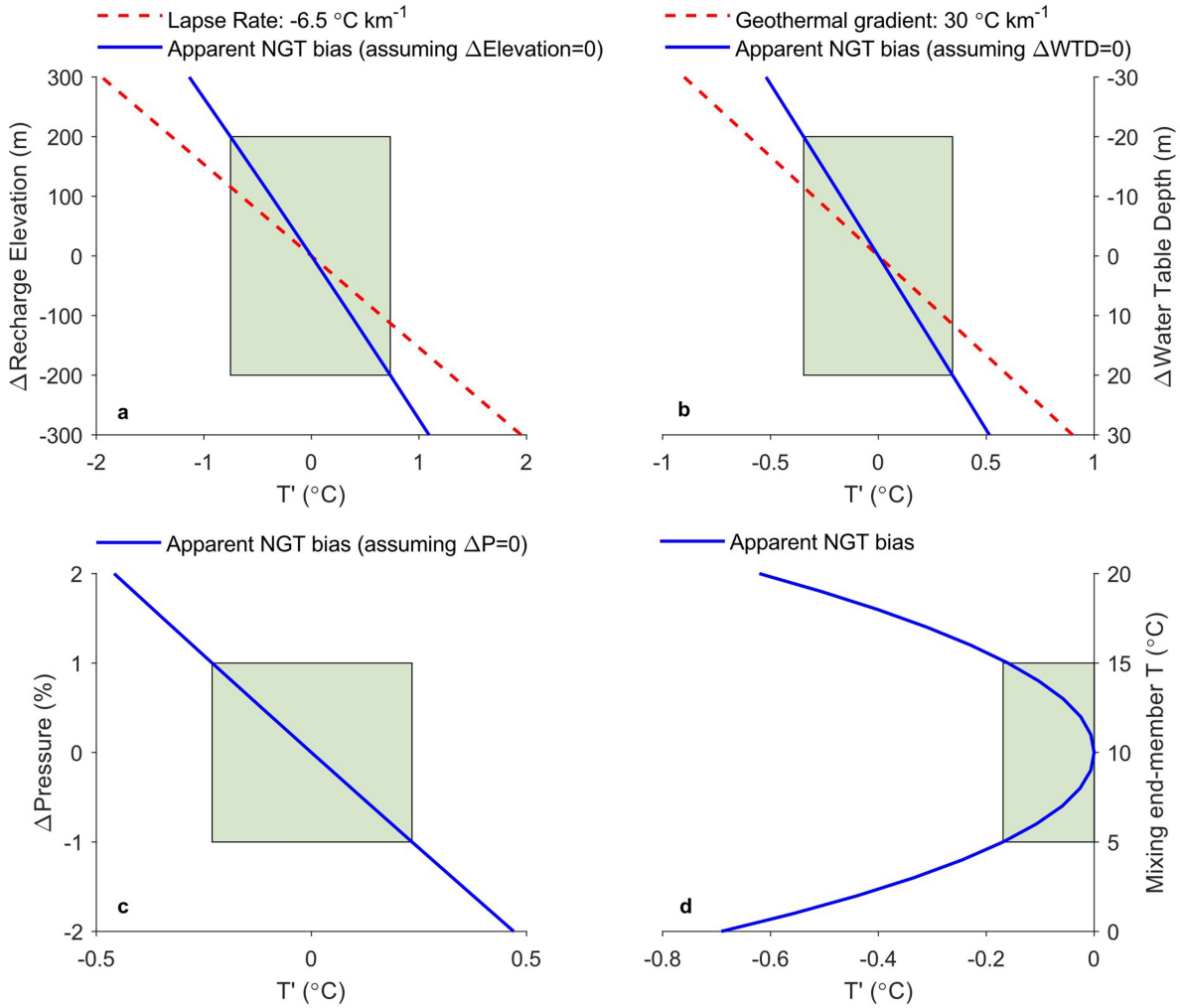

Extended Data Fig. 3 | Leading sources of systematic error in LGM noble gas palaeothermometry. a–**d**, Modelled sensitivity of apparent NGTs to leading sources of systematic error. In each case, NGT bias (T') is reported with respect to a starting recharge temperature of 10 °C at 1 km elevation (except for mixing tests (**d**) in which T' is given relative to the temperature of an equal-parts mixture of 10 °C equilibrated water with a given equilibrium mixing end-member temperature). The NGT bias associated with a source of error is shown, including LGM–Late-Holocene changes in recharge elevation (**a**), water table depth (ΔWTD, **b**) and pressure (ΔP, **c**), and the direct NGT bias induced by mixing (**d**) relative to the admixture temperature. Green squares indicate the ±1σ confidence region for the range of likely glacial–interglacial variability (Supplementary Table 1; see Methods for a detailed description of each sensitivity test and Supplementary Table 2 for a compilation of the results).

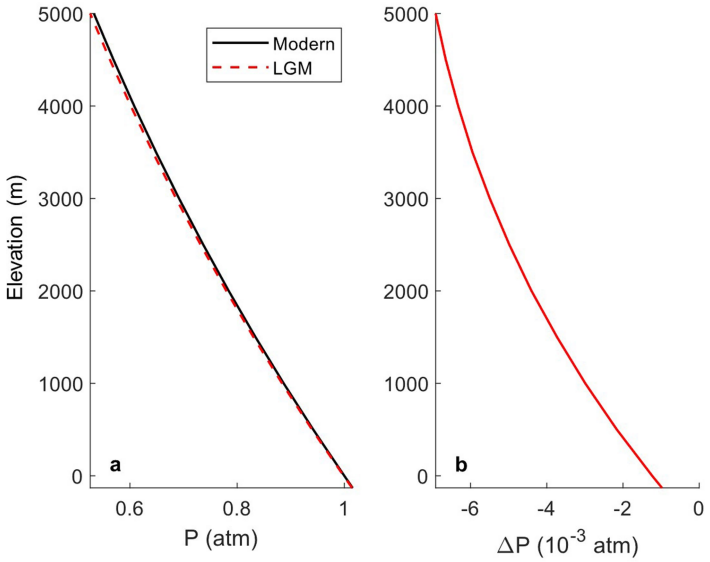

Extended Data Fig. 4 | Atmospheric pressure changes during the LGM. Box model result for changes in LGM atmospheric pressure with elevation at a fixed point. **a**, The absolute pressure (*P*) is shown during the LGM and in the modern atmosphere. **b**, LGM anomalies in pressure (ΔP) relative to the modern atmosphere are shown. In brief, the model assumes a fixed lapse rate (6.5 °C km^{-1}) and uses the barometric equation to estimate the vertical distribution of atmospheric pressure during the LGM, accounting for loss of atmospheric air by dissolution into a colder ocean and occlusion in high-latitude ice sheets, as well as displacement of air by the growth of large ice sheets (see Methods for further details).

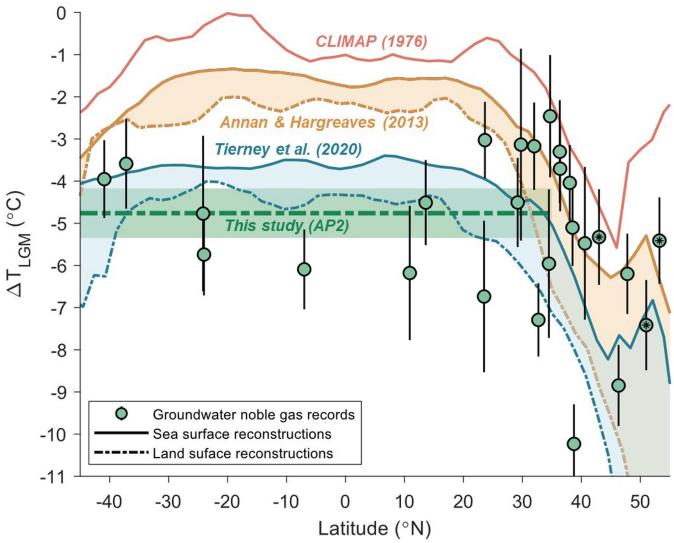

Extended Data Fig. 5 | Comparison of AP2 LGM cooling estimates to literature values. Comparison by latitude of noble-gas-derived ΔT_{LGM} (this study, approach AP2) to zonal-mean land-surface (solid lines) and sea-surface (dashed lines) estimates of ΔT_{LGM} from key previous studies[1,5,7]. Data are mean ± 1 s.e.m. Our AP2 low latitude (45° S–35° N) mean estimate of LGM cooling (4.8 ± 0.6 °C; thick green dashed line, with 95% confidence error envelope) is around 1 °C smaller in magnitude (warmer) than AP1. Although the AP2 estimate seems to more closely overlap the previously published land cooling data[1], we note that this data-assimilation study was entirely constrained by marine proxies and therefore the implications for cooling over land should be treated with caution. For the physical and statistical reasons described in the main text, we suggest that AP1 is more robust, and we emphasize that the relatively good agreement between AP1 and AP2, compared with the range of disagreement among literature values, adds confidence to the reliability of the NGT reconstruction.

Extended Data Table 1 | Leading sources of systematic error

Source of systematic error (control: 10ºC recharge temperature, 1 km elevation)	**NGT bias (T')** [±1σ]
±200-m shift in recharge elevation	-0.75 to +0.73ºC
±20-m shift in water table depth	-0.35 to +0.34ºC
±1% shift in recharge pressure	±0.23ºC
Deviation of NGT from mean recharge temperature for equal-parts binary mixing with 5ºC or 15ºC equilibrated waters	-0.17 to -0.16 ºC
Overall systematic error estimate (uncorrelated error propagation)	-0.88 to +0.85ºC

Results of sensitivity testing for systematic NGT biases in response to LGM–Late-Holocene changes in recharge elevation, water table depth and barometric pressure, in addition to the direct NGT bias induced by mixing.

Extended Data Table 2 | Overview of groundwater noble gas datasets

Citation	Latitude (ºN)	Longitude (ºE)	Recharge Elevation (m)	Late Holocene NGT (ºC)	LGM NGT, AP1 (ºC)	LGM NGT, AP2 (ºC)
Andrews and Lee 1979[63]	53.2	-0.9	90	10.1±0.3	4.0±0.7	4.7±0.4
Stute et al., 1995a[64]	36.4	-107.9	2000	9.1±0.5	3.9±0.5	5.4±0.2
Stute et al., 1995b[13]	-7.0	-41.5	450	29.3±0.2	22.5±0.4	23.2±0.3
Beyerle et al., 1998[65]	47.3	8.7	540	9.0±0.6	n/a	n/a
Clark et al., 1998[66]	38.1	-101.3	1800	13.6±0.2	n/a	n/a
Kulongoski et al., 2004[16]	-24.2	25.0	1183	23.7±1.6	17.7±0.5	18.9±0.4
Kulongoski et al., 2009[67]	34.5	-117.5	1100	n/a	11.1±0.5	12.1±0.3
Seltzer et al., 2015[68]	-40.9	173.8	116	12.4±0.3	6.8±0.4	8.5±0.2
Seltzer et al., 2019[41]	32.7	-117.1	100	21.2±0.1	13.8±0.1	14.0±0.1
Zhu and Kipfer, 2010[69]	36.3	-110.0	2025	11.4±0.7	6.7±1.0	8.1±0.5
Edmunds et al., 2006[70]	38.5	103.3	1250	11.3±0.3	5.8±0.1	6.2±0.1
Kreuzer et al., 2009[71]	38.0	115.0	108	13.8±0.2	9.1±0.2	9.7±0.2
Clark et al., 1997[59]	32.0	-82.0	100	17.4±0.4	13.1±0.5	14.3±0.4
Stute and Deak, 1989[72]	47.8	20.0	200	11.1±0.2	4.6±0.3	4.9±0.4
Beyerle et al., 2003[73]	13.6	3.7	375	32.7±0.3	27.4±0.6	28.2±0.4
Varsanyi et al., 2011[74]	46.3	20.2	112	12.7±0.4	3.5±0.3	3.8±0.2
Corcho Alvarado et al., 2009[75]	48.7	1.9	176	10.4±0.1	n/a	n/a
Blaser et al., 2010[76]	51.0	3.0	20	9.8±0.6	1.4±0.2	2.4±0.2
Klump et al., 2008[77]	43.0	-88.2	150	8.4±0.7	2.5±0.5	3.1±0.3
Aeschbach et al., 2002[37]	38.8	-76.8	50	13.9±0.3	3.7±0.2	3.7±0.2
Weyhenmeyer et al., 2000[14]	23.5	58.0	1000	31.4±1.3	24.0±1.0	24.7±0.9
Stute and Talma, 1998[78]	-24.0	19.5	1193	26.4±0.3	20.6±0.3	20.6±0.3
Saraceno et al., 2018[57]	36.7	-119.7	94	19.6±0.7	n/a	n/a
Carreira, 1998[79]	40.6	-8.7	5	14.9±1.5	9.0±0.8	9.4±0.5
This study	-37.2	140.8	120	15.3±0.6	10.4±0.4	11.7±0.3
This study	10.9	106.6	50	29.9±1.2	23.0±0.8	23.7±0.6
Stute et al., 1992[15]	29.2	-98.7	200	21.7±0.5	16.5±0.5	17.2±0.4
Masbruch et al., 2012[56]	40.6	111.6	2768	2.2±0.4	n/a	n/a
Sundal et al., 2019[80]	60.2	11.1	200	5.9±0.2	n/a	n/a
Trabelsi et al., 2019[81]	34.7	10.8	550	n/a	13.5±0.9	15.6±0.7
Abouelmagd et al., 2014[82]	29.8	34.0	761	23.0±1.6	17.6±2.0	19.8±1.3
Wieser et al., 2013[83,84]	23.6	72.3	173	28.7±0.2	23.9±0.4	25.7±0.2

Locations, recharge elevations, Late-Holocene-weighted mean NGTs and LGM NGTs (AP1 and AP2) for all datasets included in this study from previously published papers[23–26,37,41,56,57,59,63–84] and new data (this study). For further hydrogeological information, please refer to the citations associated with each dataset. Uncertainties indicate ± 1 standard (analytical) error.